

Article

Evaluation of Spoiler Model Based on Air Cooling on Lithium-Ion Battery Pack Temperature Uniformity

Chanyang Kim ¹, Jaeyoung Han ² and Seokmoo Hong ^{1,2,*} 

¹ Department of Future Convergence Engineering, Kongju National University, Cheonan 31080, Korea; white9337@smail.kongju.ac.kr

² Department of Future Automotive Engineering, Kongju National University, Cheonan 31080, Korea; hjyt11@kongju.ac.kr

* Correspondence: smhong@kongju.ac.kr; Tel.: +82-(0)41-521-9268

Abstract: Electric vehicles (EVs) and hybrid electric vehicles (HEVs) are a new trend for the vehicle industry, due to the environmental regulations of the internal combustion engine (ICE) and pollutant emission of transportation. However, despite being very promising, the durability of the battery, due to overheating, is still an obstacle. In particular, electric vehicle batteries are manufactured with high voltage and high capacity to ensure power and energy efficiency. For this reason, a high temperature is generated in the system, which reduces the battery performance and life cycle. In this study, three different layouts, based on a direct contact air-cooled system, are designed to compare and improve the cooling performance. Further, a battery cooling test is conducted to verify the designed model. The results show that the spoiler model reduces the maximum battery temperature by (about) 16%, and effectively improves the temperature distribution of the battery cell by (about) 65%, when compared with a conventional cooling method without a spoiler.

Keywords: lithium-ion battery; numerical simulation; thermal management; air cooling; spoiler model; temperature uniformity



Citation: Kim, C.; Han, J.; Hong, S. Evaluation of Spoiler Model Based on Air Cooling on Lithium-Ion Battery Pack Temperature Uniformity. *Processes* **2022**, *10*, 505. <https://doi.org/10.3390/pr10030505>

Academic Editors: Mingxia Gao and Haoran Jiang

Received: 30 December 2021

Accepted: 25 February 2022

Published: 2 March 2022

Publisher's Note: MDPI stays neutral with regard to jurisdictional claims in published maps and institutional affiliations.



Copyright: © 2022 by the authors. Licensee MDPI, Basel, Switzerland. This article is an open access article distributed under the terms and conditions of the Creative Commons Attribution (CC BY) license (<https://creativecommons.org/licenses/by/4.0/>).

1. Introduction

With the recent reinforcement of environmental regulations for internal combustion engines, more people are looking to eco-friendly electric vehicles (EVs) and hybrid electric vehicles (HEVs) [1,2]. For running an EV or HEV, a Li-ion battery system is essential. Because a series of chemical reactions occur during the use of the battery, heat generation inside the battery is unavoidable [3]. In particular, since the EV battery system has more prominent dynamic characteristics of heat generation than other battery systems, due to frequent load fluctuations, it is important to regulate the battery operating temperature consistently (20 °C to 40 °C) for stable vehicle performance [4]. In addition to performance degradation resulting from heat, the lifespan of a battery gradually decreases because of different factors, such as repeated charging and discharging, state of charge, current, and previous history, which is known as the “battery aging from use” [5,6]. Therefore, it is necessary to maintain the proper battery operating temperature, through a thermal management system, for the optimal performance and long-term durability of EVs [7,8]. Not all cylindrical batteries are applicable, but, generally, cylindrical batteries have a lower energy density than other types of battery, requiring more cells to generate high capacity, as well as extra space. Owing to such limitations, when battery cells are integrated in a narrow space, the temperature of each battery cell is higher, due to the limited air flow, than when a single cell is used [9]. Therefore, cylindrical battery cells have more spatial constraints than other types of battery cells. Battery cooling systems can be divided according to the method of heat exchange, including forced air cooling, forced water cooling, oil, other cooling methods, and phase change materials (PCMs), as shown in Figure 1 [10–14].

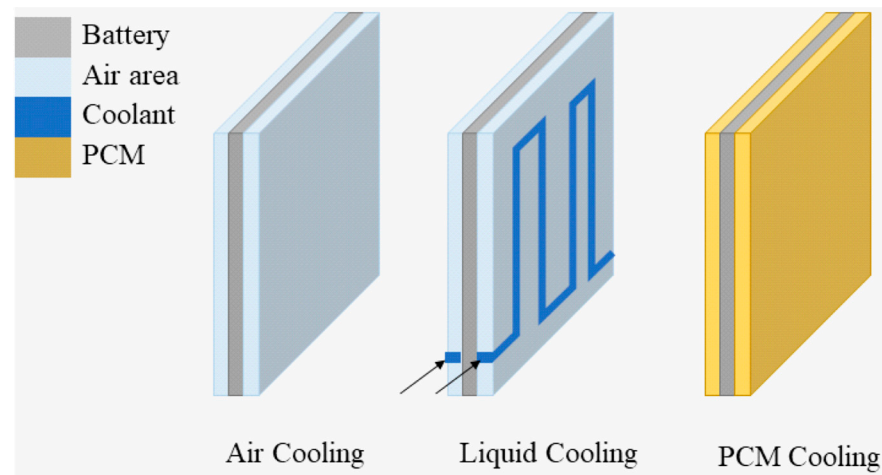


Figure 1. Types of battery cooling systems.

As shown in Figure 1, the air cooling type and the PCM type exchange heat through direct contact, while the water cooling type involves water or oil passing through channels. Extensive research has been performed on air cooling systems because of their various strengths, such as cost and low weight. Xie et al. analyzed the correlation between the fluid passage angle and cooling performance in air cooling systems, and proposed a passage angle for maximum efficiency [15]. Wang et al. assessed the cooling performance according to the number and arrangement of cells, and the location of fans and vents, and suggested the optimal cell and fan arrangement [16]. The FEA model studied by Wang et al. did not consider battery pack components other than the batteries. This can be solved by deriving the error range by conducting experiments. However, there is an uncertain aspect because there is no such process. Fan et al. analyzed the relationship between the arrangement of cells, fluid output and input temperature, and the cooling system using cylindrical battery cells [17]. By comparing the performance according to the cooling method, Chen et al. found that the air cooling type consumes the most power when the maximum temperature is controlled within a certain range [18]. Sun et al. proposed a cooling strategy to improve the temperature uniformity inside the battery pack [19]. They suggested several ducts with an optimal design and improved temperature uniformity by making a “Z-type” duct. Because the Z-type duct proposed by Sun et al. was designed using pouch-type batteries, the batteries are arranged in a straight line, producing even air flow. However, cylindrical battery cells with curved cell arrangements have uneven air flow between the cells, resulting in different temperatures around the cells [20]. Liu et al. proposed a “J-type” duct, and improved the performance of the battery pack cooling system [21]. These studies mainly focused on the maximum temperature to improve the cooling performance, while insufficient research has been conducted on constant temperature distributions. In addition, if the shape of the inlet of the air flow channel for cooling the battery is changed, it is difficult to change the design of the vehicle engine room where the batteries are installed. Any volume and weight increases are disadvantageous, in terms of fuel efficiency and the weight of the automobiles. In this study, without changing the volume of the battery pack, the cooling performance was investigated by designing a fluid passage that achieves uniform temperature distribution inside the cylindrical battery pack. For consistent cooling for a battery pack, a method was developed to increase the amount and rate of air flow in locations with higher temperatures, by using a spoiler. The weight of the battery pack case used in this study was around 1.3 kg, while the spoiler weighed about 1 g. Compared to the total weight, the weight of the spoiler was so light that it should not affect motor driving. Therefore, the design used in this study is superior, in practical terms, to previous studies on battery pack uniformity. In addition, a cooling system suitable for a cylindrical battery pack was developed and tested by simulating and comparing the cooling performances of the previously presented Z-type model and the proposed spoiler-type model.

2. Battery Simulation Modeling

2.1. Research Process

The research objective was to improve the temperature uniformity, to within the standard deviation range, by reducing the maximum temperature of the previously proposed Z-type model. When the temperature deviation was reduced to within the standard deviation, through simulation, the temperature uniformity improved by 40%, which was the goal when designing the cooling system. If the simulation result did not exceed the standard, the optimal position and length were determined by modifying the location of the spoiler. Once the improvement in the cooling performance was confirmed, using computational fluid dynamics (CFD), the validity of this study was verified with experiments.

2.2. Lumped Thermal Model for Li-Ion Battery Cell

Li-ion batteries generate the following four types of heat when being used: reaction heat, Joule's heat, polarization heat, and side reaction heat. Wan suggested Equation (1) for the process of heat generation in batteries [22].

$$q = \frac{I^2(O_{IR} + P_{IR})}{V}, \quad (1)$$

In the equation, q is the heat generation rate per unit volume, I indicates the current, O_{IR} is the ohmic internal resistance (IR) of the battery, P_{IR} is the polarization IR of the battery, and V refers to the volume of the Li-ion battery.

Wan assumed that the thermal properties of the internal material are uniform in a battery heat transfer simulation study, and that uniform heat is generated in each part of the battery by ignoring the convection and radiant heat transfer occurring between solid and liquid materials, and maintaining the internal current balance [22]. Therefore, through this assumption in this study, the battery thermal model was assumed to be a lumped capacity method to reduce the computational load.

2.3. Battery Pack Modeling

The battery model applied in this study consisted of 27 cells of the 18650 cylindrical lithium-ion battery, and Figures 2 and 3 show the specifications of the exterior case, interior design, and battery pack. The battery cells were arranged in nine rows in an in-line tube bank form.

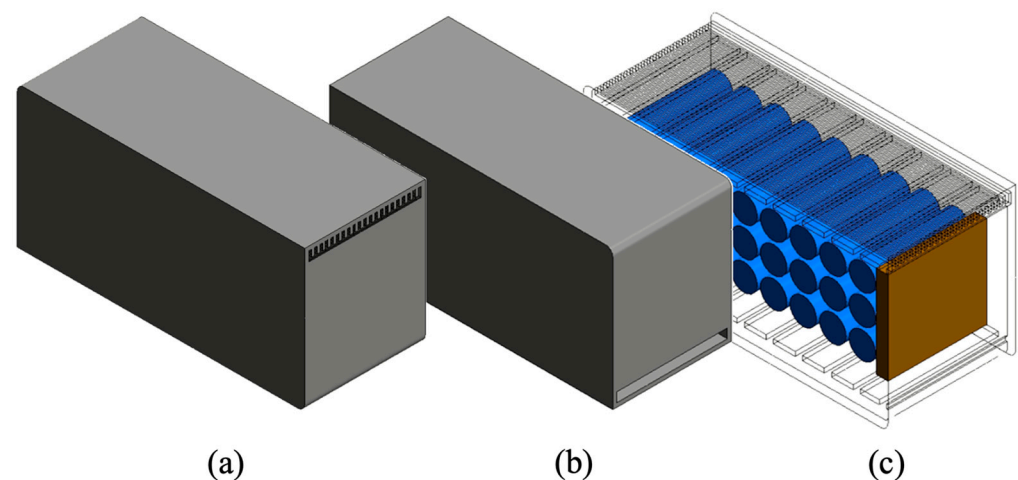


Figure 2. (a) Isometric view towards the exit; (b) isometric view towards the entrance; (c) inside the battery pack.

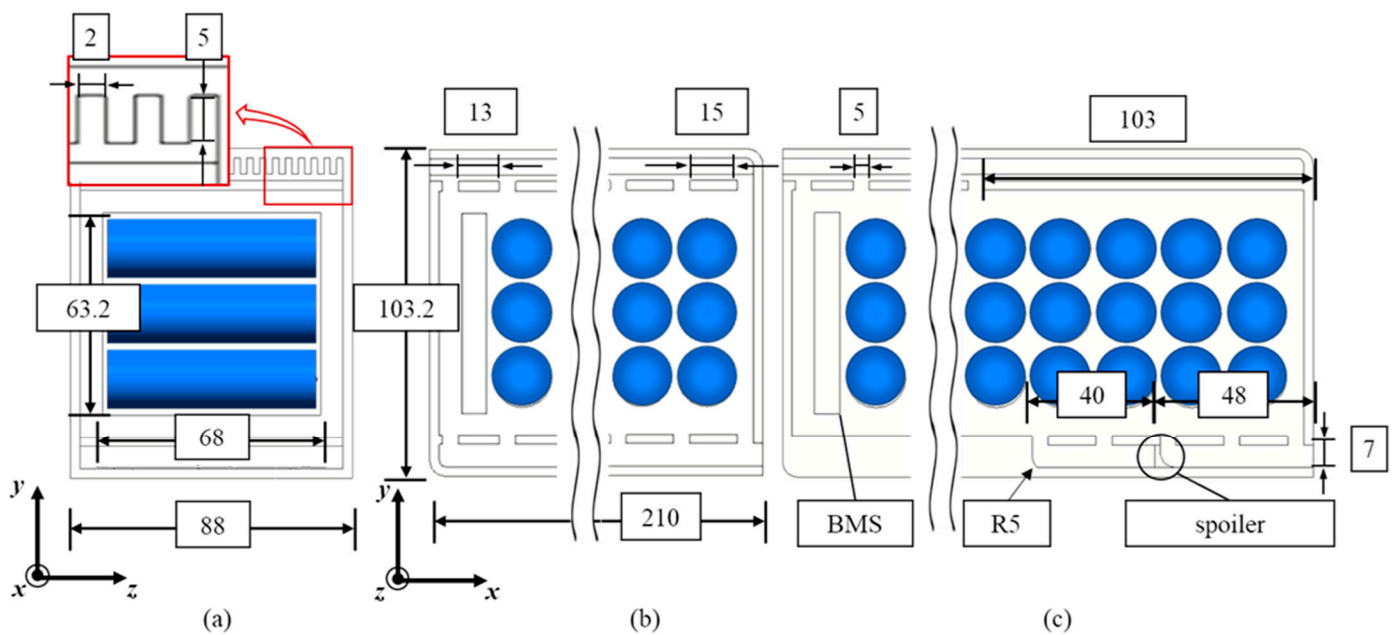


Figure 3. Configurations of the battery pack system: (a) front view; (b) top view of Z-type model; (c) top view of spoiler-type model.

A battery management system (BMS) was installed at the outlet of the cooling channel to minimize friction loss in the cooling air flow. Three different layouts, i.e., the Z-type cooling path model, a model with a heatsink at the outlet, and the spoiler-type model proposed in this study, were applied to compare and improve the cooling performance. For the Z-type model, the inlet and outlet air flow channels are located diagonally in the battery case. In addition, the air flow channels are 5 mm in size and are situated at intervals of 15 mm for uniform air distribution to the battery cell. Moreover, the last interval at the channel outlet is 13 mm. The ‘Heatsink model’ employs a series of 5 mm deep grooves, manufactured at 2 mm intervals, in a heatsink shape, at the flow path outlet of the Z-type model. Finally, the airflow improvement model presented in this study employs a small ‘spoiler’ for airflow control that is additionally installed in the ‘Heatsink model’. Two spoilers were installed in the systems. The first had a height of 7 mm and a length of 40 mm, and was located 48 mm away from the entrance of the cooling channel, to change the air flow into the battery cell; the second spoiler was installed 98 mm away from the cooling channel entrance, so that air flowing in the x-direction was directed into the y-direction. The spoilers were designed with a curved surface to minimize the coefficient of friction for the inflow air.

2.4. Numerical Method

CFD simulation was performed using ANSYS Fluent 2021 R1. The energy, momentum, and continuity equations commonly used for CFD are as follows:

$$\frac{\partial}{\partial t} \left(\rho \left(e + \frac{v^2}{2} \right) \right) + \nabla \cdot \left(\rho v \left(h + \frac{v^2}{2} \right) \right) = \nabla \cdot \left(k_{eff} \nabla T - \sum_j h_j \vec{J}_j + \vec{\tau}_{eff} \cdot \vec{v} \right) + S_h \quad (2)$$

where k_{eff} is the effective conductivity and \vec{J}_j is the diffusion flux for j . The first three terms on the right side of Equation (2) represent conduction, diffusion, and energy transfer to viscous dissipation, respectively. In Equation (2), enthalpy h is defined as an ideal gas. For incompressible materials, the pressure value is included, as shown in Equation (3). In this equation, Y_j is the mass fraction for j , the sensible heat for h_j is part of enthalpy, only

including the enthalpy change resulting from specific heat, p indicates the pressure, and ρ is the density.

$$h = \sum_j Y_j h_j + \frac{p}{\rho} \quad (3)$$

Equation (4) is a mass conservation equation, where S_m is the mass added or lost.

$$\frac{\partial \rho}{\partial t} + \nabla \cdot (\rho \vec{v}) = S_m \quad (4)$$

Equation (5) is the momentum equation, where $\rho \vec{g}$ is gravity and \vec{F} is external force.

$$\frac{\partial}{\partial t} (\rho \vec{v}) + \nabla \cdot (\rho \vec{v} \vec{v}) = -\nabla p + \nabla \cdot (\vec{\tau}) + \rho \vec{g} + \vec{F} \quad (5)$$

In this study, the most popular model of k - ϵ turbulence was used. Proposed by Launder and Spalding, this model has most commonly been used for calculating turbulence [23]. Because, in this study, only flow rates were considered for the air inflow condition, the standard k - ϵ model was used, and the equations are shown in Equations (6) and (7), where k is the turbulent kinetic energy, G_k indicates the generation of turbulent kinetic energy resulting from the mean velocity gradients, G_b is the generation of turbulent kinetic energy caused by buoyancy, Y_m is the contribution of the fluctuating dilatation in compressible turbulence to the overall dissipation rate, σ_k is the turbulent Prandtl number for k , σ_ϵ is the turbulent Prandtl number for ϵ , and S is the source term.

$$\frac{\partial}{\partial t} (\rho k) + \frac{\partial}{\partial x_i} (\rho k u_i) = \frac{\partial}{\partial x_j} \left[\left(u + \frac{u_t}{\sigma_k} \right) \frac{\partial k}{\partial x_j} \right] + G_k + G_b - \rho \epsilon - Y_M + S_k \quad (6)$$

$$\frac{\partial}{\partial t} (\rho \epsilon) + \frac{\partial}{\partial x_i} (\rho \epsilon u_i) = \frac{\partial}{\partial x_j} \left[\left(u + \frac{u_t}{\sigma_\epsilon} \right) \frac{\partial \epsilon}{\partial x_j} \right] + C_{1\epsilon} \frac{\epsilon}{k} (G_k + C_{3\epsilon} G_b) - C_{2\epsilon} \rho \frac{\epsilon^2}{k} + S_\epsilon \quad (7)$$

2.5. Simulation Mesh and Boundary Conditions

To create a simulation mesh, ANSYS Mesh was used. Because creating a mesh is important for an accurate simulation, ANSYS Mesh linked with ANSYS Fluent (www.ansys.com/products/fluids/ansys-fluent, accessed on 1 December 2021) was used.

The number of generated elements was approximately 450,000, which is shown in Figure 4. During the simulation, the physical properties of aluminum were used for both the battery and the battery pack case, and the values are shown in Table 1. The cylindrical battery cells were made with aluminum cans, and the battery pack case was made of aluminum for thermal conductivity, durability, and a light weight. For the air flowing into the inlet to cool the battery cells, an inflow rate of 10 m/s and a flow temperature of 25 °C were set under the condition of using a blower with a maximum flow rate of 21 m³/h. For the outlet, air was free to flow in and out. In this study, the amount of heat generated by the battery cells was assumed to be normal, and was set to 17,700 W/m³, considering the characteristics of the battery described in Equation (1) and Table 2. The generated heat was cooled by convection with the outside air and convective heat transfer with the incoming air.

Table 1. Material properties of Al6061.

Parameter	Value
Density [kg/m ³]	2719
Specific Heat [J/(kgK)]	871
Thermal Conductivity [W/(mK)]	202.4

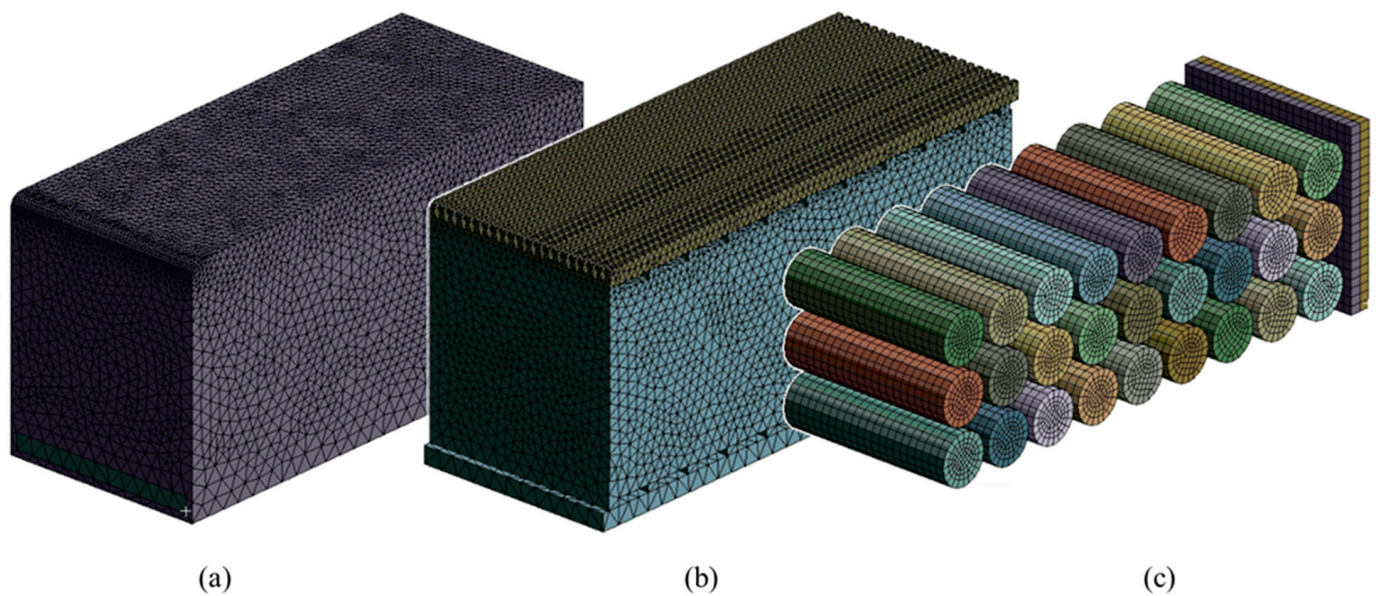


Figure 4. Configurations of CFD mesh: (a) battery pack case; (b) fluid area and exhaust heatsink; (c) battery cell and BMS.

Table 2. Specifications of the 18650 battery cell used in this study.

Parameter	Value
Nominal Capacity	2600 mAh (0.2 C, 2.75 V discharge)
Minimum Capacity	2550 mAh (0.2 C, 2.75 V discharge)
Charging Voltage	4.2 ± 0.05 V
Nominal Voltage	3.7 V
Charging Method	CC-CV
Max. Charge Current	2600 mA (ambient temperature 25 °C)
Max. Discharge Current	5200 mA (ambient temperature 25 °C)
Discharge Cut-off Voltage	2.75 V
Cell Weight	47.0 g max
Cell Dimension	Height: 65 mm max, diameter: 18.40 mm max

3. CFD Simulation Results and Discussion

The heat transfer coefficients used for convection and outside air temperature were assumed to be natural convection with air, and were set to $5 \text{ W/m}\cdot\text{K}$ and $25 \text{ }^\circ\text{C}$, respectively. A simulation using the “coupled” solution method, which obtains a strong and efficient single-phase implementation for a steady-state flow [24], was performed.

The result was calculated by Ansys software using an NVIDIA DGX Station (Future Automotive Intelligent Electronics Core Technology Center, Cheonan, Korea).

3.1. Simulation Result 1: Temperature Distribution

Figure 5 shows the simulation results of the battery pack designed in this study. Figure 5a shows the Z-type cooling model, Figure 5b shows the heatsink model, Figure 5c shows the spoiler-type model. A maximum temperature of $34.54 \text{ }^\circ\text{C}$ was observed for cell 7 in the Z-type model, and a maximum temperature of $33.76 \text{ }^\circ\text{C}$ was observed for cell 6 in the heatsink model. The heatsink and Z-type models had the same air flow amount and rate in the battery cells. For this reason, the Reynolds number was the same, as was the heat transfer coefficient inside the cells. However, because the addition of the heatsink model increases the area of heat transfer compared to the Z-type model, the heatsink model shows similar temperature distribution to that of the Z-type model, but the cooling effects for cells 4, 5, 6, 7, and 8 were improved. In Figure 5b, the temperatures of cells 15 and 16 of the Z-type model were lower than those of nearby cells. In general, the temperature of the

central cell should be high because of the conduction between cells, but a large amount of air flows towards cells 15 and 16, resulting in more impact from convection than from conduction. A more detailed discussion is provided in Section 3.2.

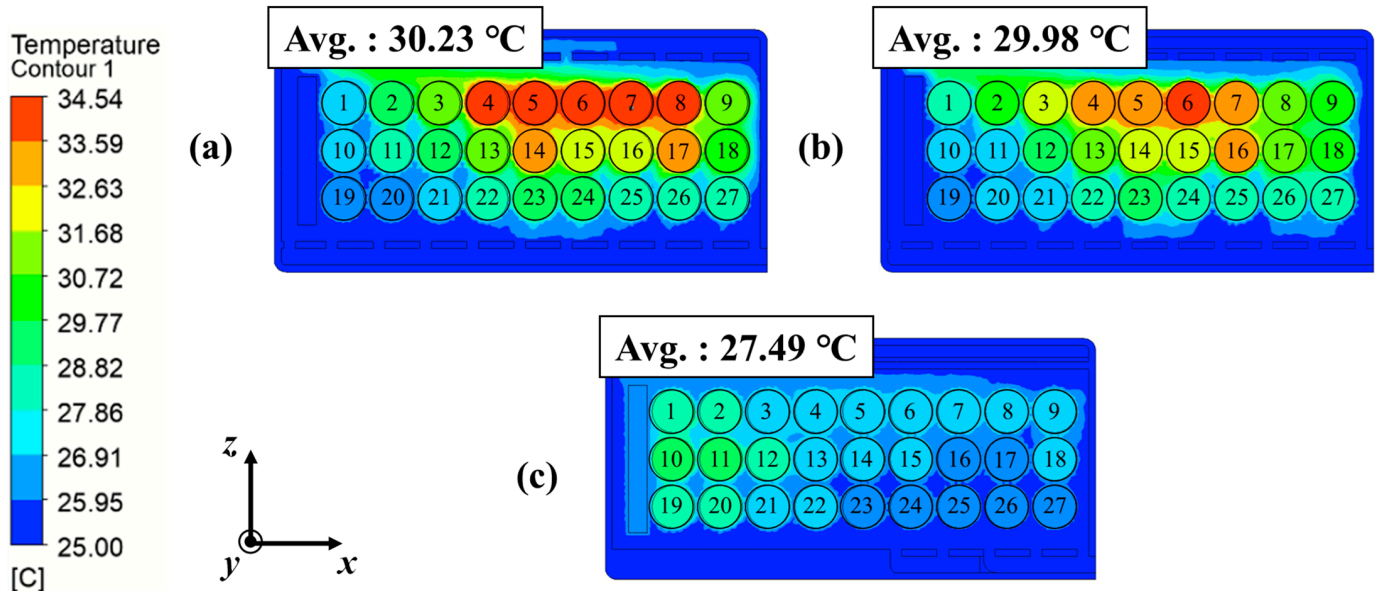


Figure 5. Temperature distribution on top of the module with different air cooling systems: (a) Z-type model; (b) heatsink model; (c) spoiler-type model.

For quantitative data analysis, Figure 6 shows the cell temperature values of all the models compared. When the average temperatures of the Z-type and heatsink models were compared, the latter model was 0.25 °C lower, but it is difficult to conclude that this was an effective improvement in cooling. However, the average temperature of the spoiler-type model improved by 9% to 27.5 °C. The maximum temperature was 29.01 °C in cell 10, showing a 16% improvement when compared with the Z-type model. The largest difference in the temperature of the battery cells was 2.78 °C, which was 5.29 °C lower, and an approximately 65.5% improvement, compared with the Z-type model. In addition, the standard deviation improved by 72%, from 2.58 °C to 0.73 °C. A comparison between cells 10 and 19 revealed that the spoiler-type model had higher temperatures than the Z-type model. In other words, the average temperature decreased through air flow improvement, but the average temperature decrease was smaller than the maximum temperature decrease resulting from cells whose temperatures increased more than those in the existing model. Even though the temperatures of cells 10 and 19 were slightly higher, the maximum temperature of the spoiler-type model was lower than the average temperature of the Z-type model. Thus, the spoiler-type model yielded better results for carrying out effective cooling, with respect to maximum temperature and temperature uniformity. That is why temperature distribution was analyzed with the air flow inside the battery pack.

3.2. Simulation Result 2: Velocity Distribution

Figure 7 shows the amount and rate of air flow inside the battery pack to analyze the cause of the temperature distribution change. In the Z-type and heatsink models, air flowed from the inlet, through the passage near cell 19, to the outlet, so more air passed through cells 1, 10, 19, and 20. This increased the Reynolds number and heat transfer coefficient, improving the cooling efficiency. Because the amount of air flow inside the battery varied depending on the location of the spoiler, it was placed in such a way as to increase the flow of air towards cells 6 and 7, where the temperature was high. Accordingly, the cooling uniformity was improved by increasing the Reynolds number for cells 5, 6, and 7.

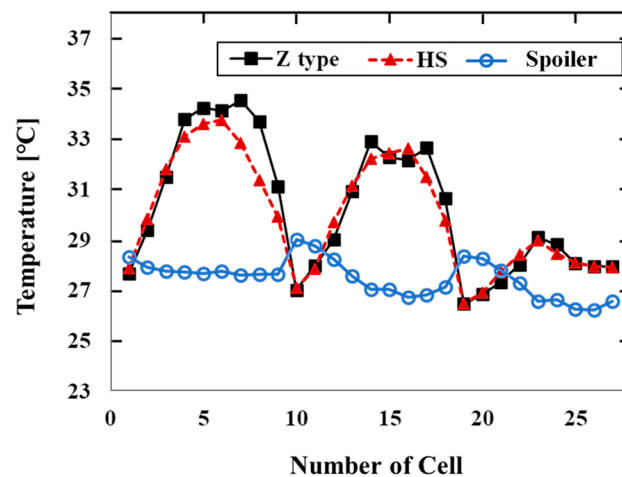


Figure 6. Temperature distribution of battery cells with cell number.

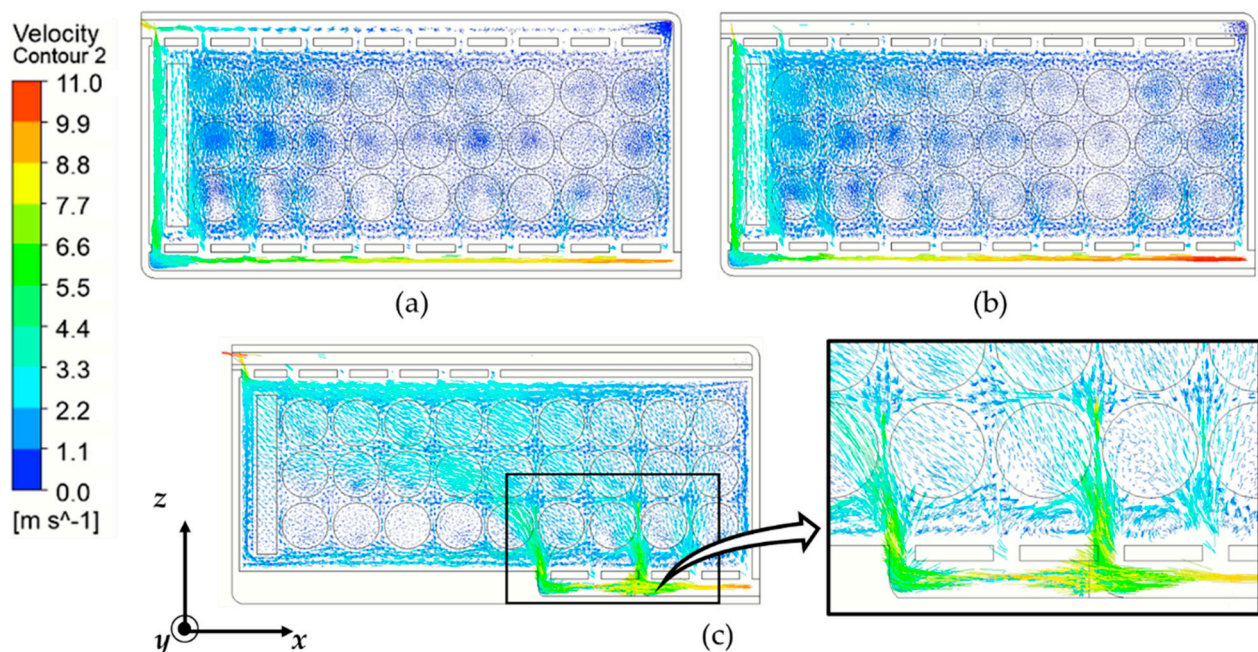


Figure 7. Velocity contours of airflow rate in the battery pack: (a) Z-type model; (b) heatsink model; (c) spoiler-type model.

As shown in Figure 7c, the air flow changed between cells 25 and 26, when the spoiler was installed near the inlet. For the air flow distribution of the Z-type and heatsink models, the air flow between cells 14 and 17 was slower than 1 m/s, and little air flow was found. In the spoiler-type model, however, the maximum flow rate at the same location was 3.3 m/s, indicating that air flowed smoothly between the battery cells. This helped improve the uniformity of the battery pack temperature.

4. Battery Cooling Experiment for Model Verification

4.1. Experimental Set Up

The developed spoiler-type model was validated in a real system. The test settings for examining the battery pack designed in this study are shown in Figure 8. The battery pack case was made of aluminum, and the electrode tabs of the battery cells were protected by a plastic case for insulation. In addition, plastic insulation was used between the BMS and the battery cells to reduce the impact of heat generated from the BMS and the electric wires, and the wires were set along the plastic case. The battery pack case and fluid passage

were manufactured according to the dimensions shown in Figure 3, and they were tested. An FLIR E53 thermal imaging camera (FLIR Systems, Wilsonville, OR, USA) was used to measure the battery temperature (detailed specifications are shown in Table 3. To create the condition of thermal equilibrium between the battery cell temperature before discharge, after a full charge, and the surrounding temperature, the battery was discharged after approximately 1 h. The battery was discharged from the full charge voltage of 12.5 V to the full discharge voltage of 8.4 V using a discharge current of 20 A, the maximum discharge current. Since the surrounding temperature was 19 °C during the test, the test results were compared with the results of another simulation, in which the surrounding temperature of 25 °C was reset to 19 °C.



Figure 8. Schematics of the experimental system for the spoiler-type model: (a) inside the model; (b) schematic of assembled battery module; (c) outside the model; (d) with the spoiler at the inlet.

Table 3. Specifications of the FLIR E53 thermal imaging camera.

Parameters	Value
IR Resolution	240 × 180 (43,200 pixels)
Object Temperature Range	−20 to 120 °C (−4 to 248 °F) 0 to 650 °C (32 to 1200 °F)
Detector Type and Pitch	Uncooled microbolometer, 17 μm
Thermal Sensitivity/NETD	<0.04 °C @ 30 °C (86 °F), 24 mm lens
Spectral Range	7.5 to 14.0 μm
Image Frequency	30 Hz
Field of View (FOV)	24 mm × 18 mm (18 mm lens)
F-Number	f/1.3

4.2. Experiment Result

Figure 9 shows the results of testing the performance of the spoiler-type cooling system and the analysis results. The maximum and minimum values of the left and right sides of the battery pack were measured with an infrared camera, and these values were compared with the simulation results. For the temperature distribution, the simulation results were in line with the test results. The maximum and minimum values of the left and right sides shown in Figure 9a,b were compared with the experimental results Figure 9c,d to investigate the quantitative accuracy of the simulation results, and the results are shown in Figure 10. The error bar indicates a range of 5%.

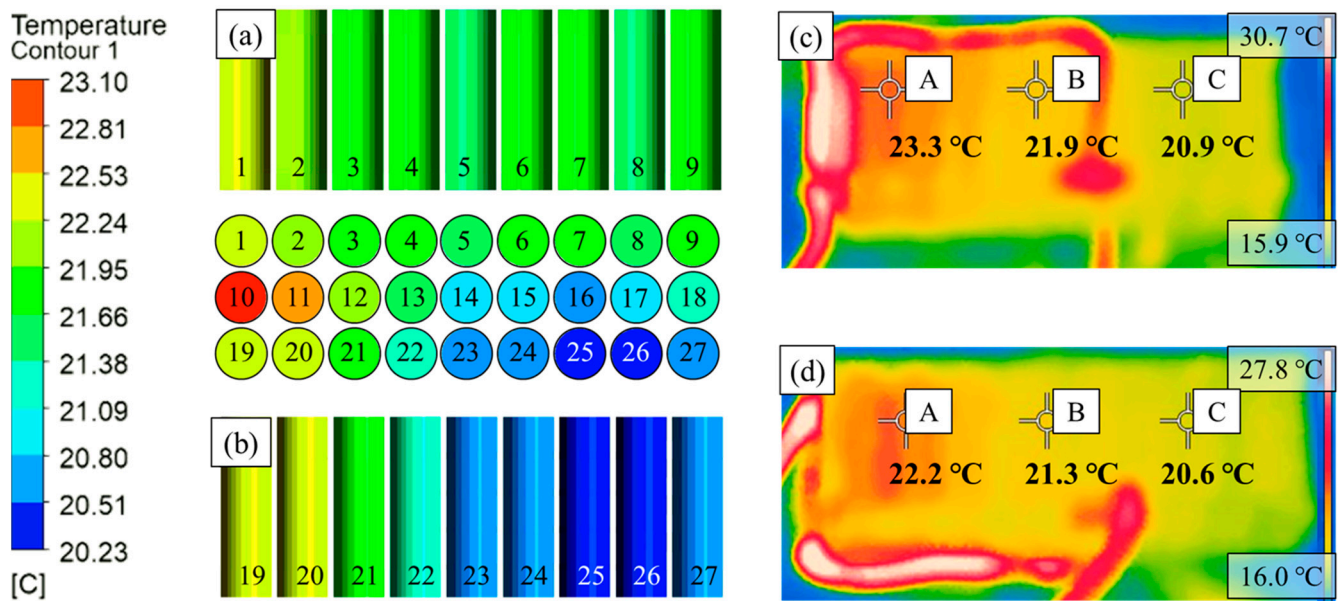


Figure 9. Simulation and experiment results for model verification: (a) simulation right view; (b) simulation left view; (c) experiment right view; (d) experiment left view.

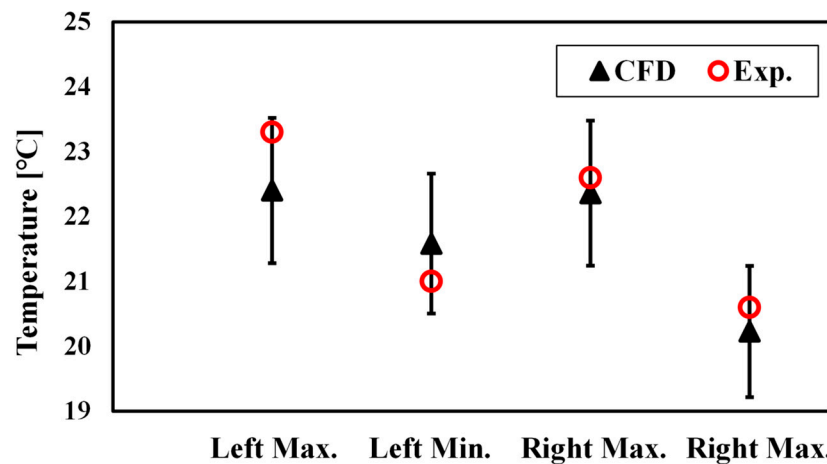


Figure 10. Comparison of maximum/minimum temperature between simulation and experiment.

The maximum temperature measured in the experiment was approximately 23.3 °C, with an error of approximately 4%, while the error of the minimum value of the right side was approximately 1%. According to the experiment, heat was generated in the BMS and the wires, which led to a higher temperature compared to the simulation, but it was still within the error range. Considering such errors, the proposed spoiler-type model is superior, based on the data obtained from the actual experiment. In addition, the spoiler model proposed in this study has an advantage in terms of weight. The battery pack used in a Tesla weighs about 450 kg and uses 6800 cells, so the case alone weighs about 130 kg [25]. Considering that the weight of the spoiler used in this study was 1/1000 of the weight of the case, there is the promise that it can improve the performance of the battery with about 1 kg of parts. However, the battery pack used in this study was not the actual capacity used in vehicles, but a smaller type of battery pack, manufactured simply. Therefore, additional research is necessary to apply it to an actual scale model. At this time, by using the design presented in this study, it is possible to design a battery pack with excellent performance, battery efficiency, and a light weight.

The temperature distributions of battery modules vary with different numbers, arrangements, and distances of battery cells; therefore, it is necessary to employ the simulation

method used in this study to explore the cooling performance [22]. The 3S9P type used in this study had the maximum temperature in cells 6 and 7, where the spoiler was installed. Therefore, if the maximum temperature occurs in a different cell, the optimal location can be found with a simulation, instead of using the same spoiler location as in this study. By changing the air flow with a spoiler, as in this study, the battery cooling system can be improved effectively.

5. Conclusions

In this study, three different cooling layouts were designed based on a direct contact air-cooled system. A flow path design with a spoiler was proposed to maintain the temperature uniformity of the cells in the battery pack. To analyze the effect of cooling performance, according to the flow path design, the spoiler-type model was compared with the basic Z-type model and the heatsink model.

- (1) In a comparison of the spoiler-type cooling system with the Z-type model, the maximum temperature difference of the battery cells improved by approximately 65.5%, from 8.07 °C to 2.78 °C, and that inside the battery pack improved by approximately 14%, from 32.94 °C to 28.28 °C.
- (2) It is clear that the proposed spoiler-type model matched the experimental data very well, since the maximum relative error was less than 4%. Therefore, the proposed spoiler-type model reproduces real battery cooling system characteristics with sufficient precision.
- (3) Further research is required to apply the basic battery pack used in this study to an actual scale model, in which case-efficient research will be possible if the method developed in this study is used.
- (4) Finally, we obtained results that the spoiler-type model performs better for achieving a higher cooling effect. Therefore, in order to use the spoiler-type model, the shape and location of the spoiler should be considered, because the spoiler cooling method depends upon the number and arrangement of the battery cells.

Author Contributions: Conceptualization, S.H.; data curation, C.K. and J.H.; investigation, C.K.; methodology, C.K., J.H. and S.H.; project administration, S.H.; software, C.K.; supervision, S.H.; validation, C.K.; visualization, C.K.; writing—original draft, C.K. and J.H.; writing—review & editing, S.H. All authors have read and agreed to the published version of the manuscript.

Funding: This study was supported by “Regional Innovation Strategy (RIS)” through the National Research Foundation of Korea (NRF) funded by the Ministry of Education (MOE)(2021RIS-004).

Institutional Review Board Statement: Not applicable.

Informed Consent Statement: Not applicable.

Data Availability Statement: The data presented in this study are available in article.

Conflicts of Interest: The authors declare no conflict of interest.

References

1. Liu, R.; Chen, J.; Xun, J.; Jiao, K.; Du, Q. Numerical investigation of thermal behaviors in lithium-ion battery stack discharge. *Appl. Energy* **2014**, *132*, 288–297. [[CrossRef](#)]
2. Ahmadi, S.; Bathaee, S.M.T.; Hosseinpour, A.H. Improving fuel economy and performance of a fuel-cell hybrid electric vehicle (fuel-cell, battery, and ultra-capacitor) using optimized energy management strategy. *Energy Convers. Manag.* **2018**, *160*, 74–84. [[CrossRef](#)]
3. Smith, K.; Wang, C.Y. Power and thermal characterization of a lithium-ion battery pack for hybrid-electric vehicles. *J. Power Source* **2006**, *160*, 662–673. [[CrossRef](#)]
4. Lu, Z.; Yu, X.L.; Wei, L.C.; Cao, F.; Zhang, L.Y.; Meng, X.Z.; Jin, L.W. A comprehensive experimental study on temperature-dependent performance of lithium-ion battery. *Appl. Therm. Eng.* **2019**, *158*, 113800. [[CrossRef](#)]
5. Wang, J.; Liu, P.; Hicks-Garner, J.; Sherman, E.; Soukiazian, S.; Verbrugge, M.; Tataria, H.; Musser, J.; Finamore, P. Cycle-life model for graphite-LiFePO₄ cells. *J. Power Source* **2011**, *196*, 3942–3948. [[CrossRef](#)]

6. Waag, W.; Käbitz, S.; Sauer, D.U. Experimental investigation of the lithium-ion battery impedance characteristic at various conditions and aging states and its influence on the application. *Appl. Energy* **2013**, *102*, 885–897. [[CrossRef](#)]
7. Han, X.; Ouyang, M.; Lu, L.; Li, J.; Zheng, Y.; Li, Z. A comparative study of commercial lithium ion battery cycle life in electrical vehicle: Aging mechanism identification. *J. Power Source* **2014**, *251*, 38–54. [[CrossRef](#)]
8. Giuliano, M.R.; Advani, S.G.; Prasad, A.K. Thermal analysis and management of lithium–titanate batteries. *J. Power Source* **2011**, *196*, 6517–6524. [[CrossRef](#)]
9. Ye, Y.; Shi, Y.; Cai, N.; Lee, J.; He, X. Electro-thermal modeling and experimental validation for lithium ion battery. *J. Power Source* **2012**, *199*, 227–238. [[CrossRef](#)]
10. Reyes-Marambio, J.; Moser, F.; Gana, F.; Severino, B.; Calderón-Muñoz, W.R.; Palma-Behnke, R.; Cortés, M. A fractal time thermal model for predicting the surface temperature of air-cooled cylindrical Li-ion cells based on experimental measurements. *J. Power Source* **2016**, *306*, 636–645. [[CrossRef](#)]
11. Li, K.; Yan, J.; Chen, H.; Wang, Q. Water cooling based strategy for lithium ion battery pack dynamic cycling for thermal management system. *Appl. Therm. Eng.* **2018**, *132*, 575–585. [[CrossRef](#)]
12. Ling, Z.; Wang, F.; Fang, X.; Gao, X.; Zhang, Z. A hybrid thermal management system for lithium ion batteries combining phase change materials with forced-air cooling. *Appl. Energy* **2015**, *148*, 403–409. [[CrossRef](#)]
13. Khateeb, S.A.; Amiruddin, S.; Farid, M.; Selman, J.R.; Al-Hallaj, S. Thermal management of Li-ion battery with phase change material for electric scooters: Experimental validation. *J. Power Source* **2005**, *142*, 345–353. [[CrossRef](#)]
14. Xie, J.; Ge, Z.; Zang, M.; Wang, S. Structural optimization of lithium-ion battery pack with forced air cooling system. *Appl. Therm. Eng.* **2017**, *126*, 583–593. [[CrossRef](#)]
15. Zhao, R.; Gu, J.; Liu, J. An experimental study of heat pipe thermal management system with wet cooling method for lithium ion batteries. *J. Power Source* **2015**, *273*, 1089–1097. [[CrossRef](#)]
16. Wang, T.; Tseng, K.J.; Zhao, J.; Wei, Z. Thermal investigation of lithium-ion battery module with different cell arrangement structures and forced air-cooling strategies. *Appl. Energy* **2014**, *134*, 229–238. [[CrossRef](#)]
17. Fan, Y.; Bao, Y.; Ling, C.; Chu, Y.; Tan, X.; Yang, S. Experimental study on the thermal management performance of air cooling for high energy density cylindrical lithium-ion batteries. *Appl. Therm. Eng.* **2019**, *155*, 96–109. [[CrossRef](#)]
18. Chen, D.; Jiang, J.; Kim, G.H.; Yang, C.; Pesaran, A. Comparison of different cooling methods for lithium ion battery cells. *Appl. Therm. Eng.* **2016**, *94*, 846–854. [[CrossRef](#)]
19. Sun, H.; Dixon, R. Development of cooling strategy for an air cooled lithium-ion battery pack. *J. Power Source* **2014**, *272*, 404–414. [[CrossRef](#)]
20. Yang, N.; Zhang, X.; Li, G.; Hua, D. Assessment of the forced air-cooling performance for cylindrical lithium-ion battery packs: A comparative analysis between aligned and staggered cell arrangements. *Appl. Therm. Eng.* **2015**, *80*, 55–65. [[CrossRef](#)]
21. Liu, Y.; Zhang, J. Design a J-type air-based battery thermal management system through surrogate-based optimization. *Appl. Energy* **2019**, *252*, 113426. [[CrossRef](#)]
22. Wan, C. Battery space optimization to limit heat transfer in a lithium-ion battery using adaptive elephant herding optimization. *Ionics* **2020**, *26*, 4993–5009. [[CrossRef](#)]
23. Launder, B.E.; Spalding, D.B. *Lectures in Mathematical Models of Turbulence*; Academic Press: New York, NY, USA, 1972.
24. Fluent, A. *Ansys Fluent Theory Guide*; ANSYS INC.: Canonsburg, PA, USA, 2021; Volume 15317, pp. 919–920.
25. Berdichevsky, G.; Kelty, K.; Straubel, J.; Toomre, E. *The Tesla Roadster Battery System*; Tesla Motors: Palo Alto, CA, USA, 2006.